Full Paper

Journal of the Brazilian Chemical Society

https://dx.doi.org/10.21577/0103-5053.20250043

J. Braz. Chem. Soc. **2025**, *36*, 8, e-20250043, 1-9
©2025 Sociedade Brasileira de Química

Machine Learning to Treat Data for the Design and Improvement of Electrochemical Sensors: Application for a Cancer Biomarker

Gisela Ibáñez Redín,[#,a] Daniel C. Braz,[#,a,b] Débora Gonçalves[a] and Osvaldo N. Oliveira Jr.[*,a]

[a]*Instituto de Física de São Carlos, Universidade de São Paulo (USP), 13560-970 São Carlos-SP, Brazil*

[b]*Universidade Estadual de Mato Grosso do Sul (UEMS), 79804-970 Dourados-MS, Brazil*

Label-free immunosensors based on screen-printed carbon electrodes offer a promising platform for the detection of cancer biomarkers. Herein, we explore the use of machine learning techniques to improve the performance of these immunosensors. We evaluate the influence of various redox probes on the analytical response in detecting the cancer biomarker protein p53. Ascorbic acid (AA) was found as the optimal redox probe, exhibiting a sensitivity of 0.26 ng mL^{-1}, attributed to its strong affinity to proteins through hydrogen bonds and electrostatic interactions. We also extracted analytical information from the voltammograms, such as shifts in peak potential and changes in peak width, to construct datasets for supervised machine learning. Using different algorithms including logistic regression, linear discriminant analysis, K-nearest neighbor, Gaussian Naive-Bayes, decision trees, and support vector machine, we identified positive samples spiked with p53 in artificial urine and saliva samples. Through a comparison of immunosensors with distinct molecular architectures, we determined the critical role of redox probe selection, which proves to be more significant than modifying the working electrodes in determining performance. Furthermore, immunosensors with inferior inherent detection ability can achieve comparable performance to those with superior analytical characteristics when feature selection and machine learning algorithms are applied to the voltammograms. These findings illustrate the significance of extracting additional information from differential pulse voltammograms beyond peak current intensity. Furthermore, using machine learning techniques allows one to design biosensors capable of distinguishing biomarkers even in complex samples.

Keywords: electrochemical sensors, cancer biomarker, machine learning, data analytics, redox probes

Introduction

The use of machine learning is becoming ubiquitous in tasks related to sensors and biosensors, especially to treat sensing data for enhancing sensitivity and selectivity in clinical diagnosis and monitoring the environment.[1-4] Various advantages can be highlighted with such usage, including the processing of large amounts of data, and identification of patterns on the data which allow for diagnosis in the absence of well-defined analytes or biomarkers.[2] In this context, successful examples of machine learning use are represented by data analysis in electronic tongues[5,6] and electronic noses,[7] which are devices based on pattern recognition approaches. A key feature in applying unsupervised or supervised machine learning is the ability to treat the sensing data in their entirety, as there is no limitation on the amount of data that can be processed. In electronic tongues based on electrical impedance spectroscopy, for instance, analysis with machine learning is facilitated by feature selection where the most relevant frequencies are chosen to distinguish the samples under analysis.[5] In other types of spectroscopy, such as attenuated total reflectance Fourier transform infrared spectroscopy (ATR-FTIR), the accuracy in detecting severe acute respiratory syndrome coronavirus 2 (SARS-CoV-2) infection is enhanced by treating the whole spectra (or selected parts) rather than specific peaks.[8] For electrochemical sensing, on the other hand, one may envisage exploiting whole voltammograms or amperograms, instead of only analyzing redox peaks or other features. While this type of analysis has been done in electrochemical electronic tongues,[9,10] only recently it has been applied to electrochemical biosensing.[11-13]

*e-mail: chu@ifsc.usp.br
[#]These authors equally contributed to this work.
Editor handled this article: Maurício Coutinho Neto (Guest)

This is an open-access article distributed under the terms of the Creative Commons Attribution License.

In this study, we conceived a set of experiments to apply machine learning to data obtained with electrochemical immunosensors for the detection of cancer biomarkers. The experiments were designed to produce balanced datasets with positive and negative cases for a biomarker, with a larger number of replications of the measurements than it is usual with electrochemical biosensors. This larger number is relevant for making it possible to use supervised machine learning. The biomarker chosen for the proof-of-principle study is the p53 tumor suppressor protein, whose quantification is important for monitoring ovarian, gastric, head, and neck cancers.[14,15] The electrochemical immunosensors made on screen-printing electrodes (SPCEs) are useful to detect analytes, including bacteria,[16] virus,[17] toxins,[18] and biomarkers in general.[1] They allow for label-free detection using antibodies immobilized on working electrodes, and by measuring the electrochemical response of a redox probe.

Herein, we compare the effect of using four probes, viz., potassium hexacyanoferrate(II), hydroquinone, hexaminerutheniun(III) chloride and ascorbic acid, on the analytical performance of electrochemical immunosensors made with SPCEs, some of which were coated with a polyethylene amine (PEI) film. A comparison of redox probes is relevant because they may undergo distinct electrochemical processes depending on the electron transfer mechanisms. While most outer sphere redox probes, such as hexaminerutheniun(III) chloride, are only slightly sensitive to functional groups attached to the electrode surface, other species such as $FeCl_3$ are highly affected by surface modification.[19] These differences can influence the type of information extracted if diverse redox probes are used for the electrochemical characterization of surfaces.[20] For example, Ferrari *et al.*[21] demonstrated that the electroactive surface area of SPCEs depends on the redox probe used, with outer sphere probes exhibiting more accurate and reliable results. The interaction with biomolecules can also vary from one redox probe to another, as reported[22] with biofouling of hexaminerutheniun, hexachloroiridate, and dopamine. These differences may affect the performance of label-free electrochemical devices and analytical parameters such as sensitivity and limit of detection. With the analysis of differential pulse voltammetry (DPV) using machine learning we can detect not only the presence of p53 in saliva and urine, but also identify the most suitable redox probe. We show that diagnosis is enhanced by considering features from the voltammograms, and not only peak current values.

Experimental

Chemicals and reagents

Bovine serum albumin (BSA), hexaminerutheniun(III) chloride ($Ru(NH_3)_6^{2+/3+}$) and hydroquinone (HQ) from Sigma-Aldrich (USA), monoclonal anti-p53 antibody (DO-7, Agilent Dako, Denmark), p53 protein (Abcam, USA), potassium hexacyanoferrate(II) ($Fe(CN)_6^{3-/4-}$) and ascorbic acid (AA) from Synth (Brazil), were used as received without purification. All solutions were prepared with ultrapure water with resistivity of 18 MΩ cm. Phosphate buffer (PB) at 0.1 mol L^{-1} (pH 7.0) was prepared using NaH_2PO_4 and Na_2HPO_4.

Fabrication of the immunosensors

SPCEs were prepared using a working electrode, a counter electrode and a Ag/AgCl reference electrode produced according to a reported procedure.[23] Prior to antibody immobilization, the working electrodes with 4 mm in diameter were electrochemically pretreated at 1.2 V *vs.* Ag/AgCl in a 0.1 mol L^{-1} NaOH solution for 300 s. Then, the electrodes were washed with water, and incubated overnight with 10 µL of anti-p53 antibodies diluted in PB pH 7.0 (1:10 v/v). To block non-specific adsorption sites, the electrodes were incubated with 10 µL of 0.1% BSA in PB for 30 min, and then washed with PB. These biosensors will be referred to as SPCE-pre/Ab/BSA. For comparison, immunosensors made with SPCEs modified with polyethyleneimine (PEI) were also prepared. The latter were produced by depositing 10 µL of solutions containing 1.0 mg mL^{-1} PEI on the pre-treated working electrode and allowed to adsorb for 30 min. The electrodes were washed with water, dried under N_2 flux, and then, coated with anti-p53 antibodies using the same protocol adopted for pre-treated SPCEs. These biosensors will be referred to as SPCE-Pre/PEI/Ab/BSA.

Electrochemical measurements

The immunosensors were incubated for 30 min with 10 µL of different concentrations of human p53 protein in PB (pH 7.0). Then, they were washed with PB and dried. The detection of p53 was monitored using DPV at a modulation time of 0.05 s, modulation amplitude of 0.09 V and potential step of 0.015 V in solutions containing 1×10^{-3} mol L^{-1} of redox probe (i.e. $Ru(NH_3)_6Cl_3$, $(Fe(CN)_6K_3$, AA or HQ) in 0.1 mol L^{-1} PB at pH 7.0. All voltammograms had their baselines corrected with the linear method in Nova software (version 2.1.4).

Analysis of p53 in artificial samples

Artificial saliva and urine samples were prepared as reported,[24] diluted 10 times using PB, and doped with known concentrations of human p53 protein. These samples were chosen to investigate the capability of detecting p53 in different matrices. The analyses were done by incubating the SPCE/Ab/BSA immunosensors with 10 μL of the sample for 30 min. The immunosensors were then washed with PB and dried. The DPV measurements were performed using the same procedures for detecting p53 in standard solutions (see sub-section "Electrochemical measurements").

Data analysis using machine learning

Datasets: the DPV data obtained from the detection of p53 in artificial urine and saliva samples were analyzed through various machine learning methods. Two different original datasets were analyzed, one for experiments made with the SPCEs-Pre (pretreated SPCE)/Ab/BSA biosensor and AA as redox probe (AA-raw), and the other with the SPCE-Pre/PEI/Ab/BSA biosensor with $Fe(CN)_6^{3-/4-}$ (PEI-raw). These two systems were chosen for machine learning-based analysis since they exhibited the best analytical performance among the possibilities tested here. Each dataset consisted of 40 voltammograms, 20 of which corresponded to measurements of negative samples (10 for saliva and 10 for urine) and 20 are from samples spiked with 0.1 ng mL^{-1} of p53 (10 for saliva and 10 for urine). Each spectrum in the dataset for AA has 81 values of current measured in the range from −400 to 800 mV, while each voltammogram for PEI has 74 points in the range from −300 to 800 mV. Three additional datasets were generated from the original data, by extracting features related to the entire voltammograms or specific characteristics of the peaks.

Table S1 (presented in Supplementary Information (SI) section) shows relevant information on each dataset. The AA-mi and PEI-mi datasets were generated from five features that provide the best distinguishability, which were selected by using mutual information. The AA-stats and PEI-stats datasets were constructed by considering statistical features from the voltammograms including mean, standard deviation, maximum, minimum, and 25, 50, 75% quartiles. The AA-peak and PEI-peak datasets were obtained using features from peak current, some of which are commonly used for analyzing electrochemical signals (i.e., position, prominence, half width, full width, and Q factor as prominence/half width).

Data visualization: dimensionality reduction and projection techniques were used to assess the ability to distinguish the two groups of samples (corresponding to positive and negative to p53) using the entire voltammograms. The techniques tested were principal component analysis (PCA),[25] neighborhood components analysis (NCA),[26] Isomap, and interactive document mapping (IDMAP).[27]

Machine learning: clustering and classification machine learning algorithms were used to discriminate between positive and negative groups. The clustering algorithms employed were K-means (KM),[28] hierarchical agglomerative clustering (HAC),[28] and spectral clustering (SC),[29] with default hyperparameters in Scikit-learn module. The average silhouette width (ASW) was used as metric to evaluate the performance, varying between −1 and +1, where values closer to +1 represent a higher clustering quality. The classification algorithms were logistic regression (LR), linear discriminant analysis (LDA), K-nearest neighbor (KNN), Gaussian Naive-Bayes (GNB), decision trees (DT), and support vector machine with linear kernel (SVML).[28] The models obtained had their performances evaluated by calculating accuracy in a leave-one-out cross-validation scheme.[23]

Results and Discussion

Analytical performance of biosensors for detecting p53 using different redox probes

The hydrophilicity of the carbon working electrode was increased by an electrochemical pretreatment, after which the anti-p53 antibodies were immobilized through passive adsorption. This pretreatment can prevent protein denaturing, also enhancing antibody immobilization[22] and the electrochemical response of SPCEs. Figure S1 (SI section) shows the cyclic voltammograms for SPCEs and SPCEs-Pre in 1.0×10^{-3} mol L^{-1} $Fe(CN)_6^{3-/4-}$ (Figure S1a), $Ru(NH_3)_6^{2+/3+}$ (Figure S1b), HQ (Figure S1c) and AA (Figure S1d). In all cases, the pretreated electrodes exhibited faster heterogeneous electron transfer rates, as inferred from the decrease in the peak-to-peak separation (ΔE_p) for *quasi*-reversible $Fe(CN)_6^{3-/4-}$, $Ru(NH_3)_6^{2+/3+}$ and HQ, and anodic peak potential (E_{pa}) for AA. This enhanced performance can be related to the removal of organic binders from the surface, which increases the number of defect sites.[30,31]

All redox probes investigated exhibited a diffusional-controlled electron transfer process on the SCPE and SPCE-Pre surfaces, according to the results with varying scan rates in Figures S2-S5 (SI section). The voltammetric response of the pretreated electrode in the presence of

redox probes was influenced by varying degrees by adsorption of anti-p53 antibodies. Figure 1 shows the cyclic voltammograms (CVs) for SPCEs-Pre before and after antibody immobilization. For the experiments with $Fe(CN)_6^{3-/4-}$ and $Ru(NH_3)_6^{2+/3+}$, the increase in ΔE_p was 48 and 35%, respectively. In the presence of HQ, the response is less sensitive, with an 18% increase in ΔE_p. The presence of AA induced an irreversible electron transfer process and an increment in E_{pa} of 27%. Different values for anodic and cathodic peak currents (I_{pa} and I_{pc}) were obtained due to a blocking process of the electrode surface, thus altering the electroactive area. Decreases in I_{pa} of 6.7, 20, and 37% were obtained for $Fe(CN)_6^{3-/4-}$, HQ and AA, respectively. In contrast, with $Ru(NH_3)_6^{2+/3+}$ there were no appreciable changes in the peak current values. The variations in the response of the redox probes, stemming from the adsorption of proteins onto the electrode, align with findings from the literature,[22] being ascribed to distinct mechanisms of electron transfer. For example, $Fe(CN)_6^{3-/4-}$ is a negatively charged inner-sphere redox probe, and highly sensitive to defects and functional groups on the electrode.[19,32] $Ru(NH_3)_6^{2+/3+}$ is considered an ideal outer-sphere redox probe. It is relatively insensitive to changes in the surface chemistry,[21] but its electrochemical response can be affected by charged materials and film thickness.[19] Organic AA and HQ probes are known to be sensitive to several factors, including surface area, density of defect sites, and presence of oxygenated species.[20] The strong interaction of AA with proteins through hydrogen bonds and electrostatic interactions[33-35] offers a plausible explanation for the high sensitivity of this probe in the voltammetric responses. It should be noticed that products of the AA oxidation reaction, such as dehydroascorbic acid and 2,3-diketogulonic acid, can adsorb onto the electrode surface potentially leading to signal loss or peak shifts.[36] Therefore, control experiments were performed to compare electrode performance after at least three consecutive voltammetric measurements in solutions containing AA with that observed after protein adsorption (antibodies and p53 protein). Minimal signal changes were observed in the absence of protein, indicating that the observed voltammetric responses are primarily attributed to protein adsorption.

We also investigated the effect of using different redox probes in the analytical parameters of label-free immunosensors. The SPCE-Pre/Ab were blocked with BSA to avoid non-specific adsorption, and then used to detect p53 protein in standard solutions. Figure 2 shows the DP voltammograms for SPCE-Pre/Ab/BSA immunosensors in 1.0×10^{-3} mol L^{-1} of $Fe(CN)_6^{3-/4-}$ (Figure 2a), $Ru(NH_3)_6^{2+/3+}$ (Figure 2b), HQ (Figure 2c) and AA (Figure 2d). For comparison purposes, immunosensors using PEI layers were also prepared to adsorb the anti-p53 antibodies (see

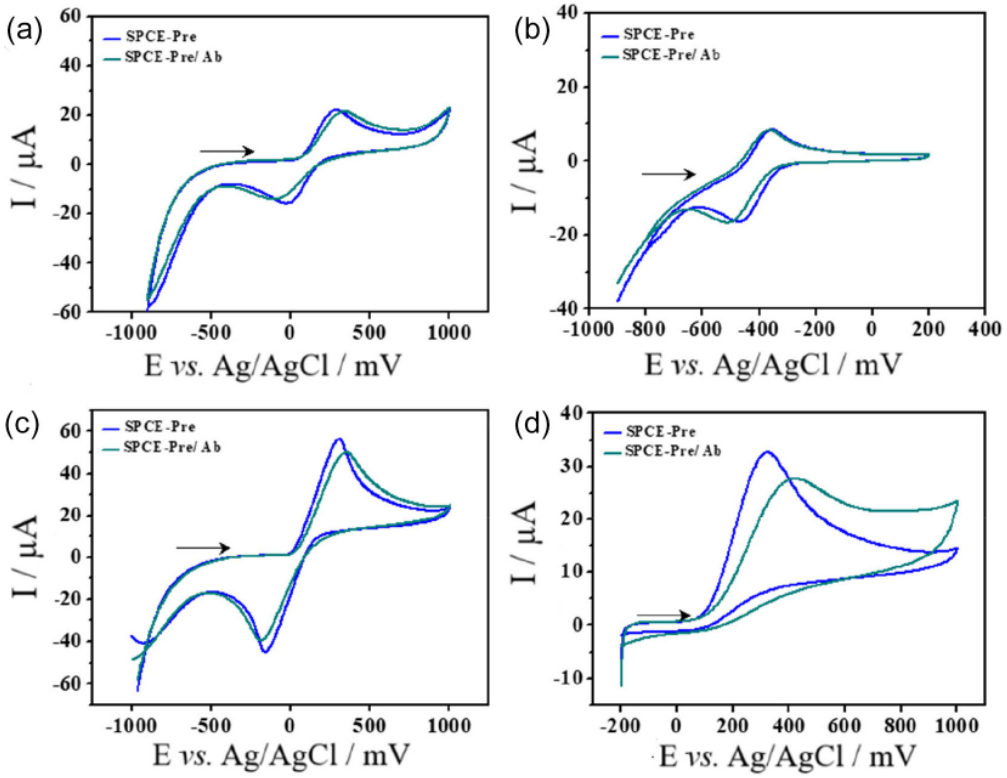

Figure 1. CVs for SPCEs-Pre before and after adsorption of anti-p53 antibodies in 1.0×10^{-3} mol L^{-1} of $K_3Fe(CN)_6$ (a), $Ru(NH_3)_6Cl_3$ (b), HQ (c) and AA (d) in 0.1 mol L^{-1} PB (pH 7). v = 100 mVs^{-1}.

sub-section "Fabrication of the immunosensors"). PEI was chosen as matrix due to its positively charged amine groups, which are known to improve both adsorption of antibodies and analytical signal of negatively-charged redox probes.[37,38] Figure 2e shows the voltammograms for the SPCE-Pre/PEI/Ab/BSA immunosensors in $Fe(CN)_6^{3-/4-}$ redox probe. The analytical curves for different systems are compared in Figure 2f. For all cases, the normalized current exhibited a linear dependence with log p53 within the concentration range from 0.01 to 1.0 ng L^{-1}, according to the following regression equations:

SPCE-Pre/Ab/BSA + $Fe(CN)_6^{3-/4-}$: $\Delta I = 0.13 \pm 0.01 + 0.054 \pm 0.009$ log p53, $r^2 = 0.967$ (1)

SPCE-Pre/Ab/BSA + $Ru(NH_3)_6^{2+/3+}$: $\Delta I = 0.206 \pm 0.005 + 0.11 \pm 0.01$ log p53, $r^2 = 0.985$ (2)

SPCE-Pre/Ab/BSA + HQ: $\Delta I = 0.105 \pm 0.002 + 0.049 \pm 0.001$ log p53, $r^2 = 0.996$ (3)

SPCE-Pre/Ab/BSA + AA: $\Delta I = 0.56 \pm 0.01 + 0.26 \pm 0.02$ log p53, $r^2 = 0.994$ (4)

SPCE-Pre/PEI/Ab/BSA + $Fe(CN)_6^{3-/4-}$: $0.312 \pm 0.008 + 0.096 \pm 0.005$ log p53 , $r^2 = 0.973$ (5)

where ΔI represents the change in current intensity for each antibody concentration relative to the blank current intensity, and r^2 is the correlation coefficient.

The analytical sensitivity of the SPCE-Pre/Ab/BSA immunosensor depends on the redox probe. The estimated sensitivities were 0.049, 0.054, 0.11 and 0.26 ng mL^{-1} for $Fe(CN)_6^{3-/4-}$, HQ, $Ru(NH_3)_6^{2+/3+}$, and AA as redox probes, respectively. The higher sensitivity of the immunosensor utilizing $Ru(NH_3)_6^{2+/3+}$ in comparison to $Fe(CN)_6^{3-/4-}$ and HQ can be due to the increased electrostatic repulsion between $Ru(NH_3)_6^{2+/3+}$ cations and positively-charged p53 (isoelectric point ranging from 7.5 to 8.0 for wild type and mutations)[39] adsorbed on the electrode. As expected from the cyclic voltammetric experiments, the analytical curves made with AA exhibited the highest sensitivity. This is attributed to the formation of a non-electroactive complex with the protein, hindering the diffusion of the redox probe to the electrode surface.[34] It is also worth noting that the analytical sensitivity of the SPCE-Pre/Ab/BSA immunosensor with AA was superior to that for the immunosensor prepared with PEI films (0.096 ng mL^{-1}). These findings illustrate the importance of selecting an optimal redox probe, as it can yield more substantial enhancements in the analytical performance compared to conventional approaches like electrode modification with functional materials.

Data analysis using information visualization and machine learning

The adsorption of insulating materials, such as proteins, on the electrodes reduces the current and may promote other relevant changes in DP voltammograms. Shifts in peak potential and increases in peak width are common in label-free electrochemical immunosensors, even with the electrodes utilized in this study (refer to Figure 2). These changes can be attributed to alterations in electron transfer kinetics[40] and have been documented in various studies.[37,41-43] While these changes in peak potential and width can be linked to the increased concentration of the analyte (protein) on the electrode, they are often overlooked during the data analysis stage when only peak current values are considered. In order to extract valuable analytical information embedded within the voltammograms, we have chosen to employ machine learning techniques. Specifically, we utilized machine learning to analyze the data obtained from the detection of p53 using the two systems that exhibited the highest sensitivities: SPCE-Pre/Ab/BSA with AA and SPCE-Pre/PEI/Ab/BSA with $Fe(CN)_6^{3-/4-}$. The data were obtained from artificial urine and saliva spiked with known concentrations of p53. Negative samples without the addition of protein were also analyzed. For each biosensor, a total of four datasets were considered, three of which were generated from the original data corresponding to the complete voltammogram of each measurement (see Table S1, SI section).

Figure 3 shows the box plot for the peak current intensity in the voltammograms for the control and spiked samples. A clear distinction is observed for the data obtained with the SPCE-Pre/Ab/BSA + AA system (Figure 3a), but not for SPCE-Pre/PEI/Ab/BSA + $Fe(CN)_6^{3-/4-}$, as some overlap occurs (Figure 3b).

Table 1 displays the clustering results using unsupervised algorithms. Overall, the AA system consistently outperformed the other ones, as anticipated due to its high sensitivity in detection. This is also consistent with the better separation between negative and positive samples in the projections of the AA-raw dataset (Figures S6 and S7, SI section). There was a noticeable improvement in clustering performance when utilizing datasets with selected features (mi, peak, and stats) instead of raw data. Box plot depicting the distribution of these features across different datasets can be found in Figures S8-S11 (SI section). For the AA system, the features associated with peak current showed significantly different distributions between positive and negative samples (see

Figure S9), potentially explaining the superior performance of clusterization when employing the AA-peak dataset. As for the PEI system, the best results were achieved using the PEI-mi dataset, which incorporates the five most influential

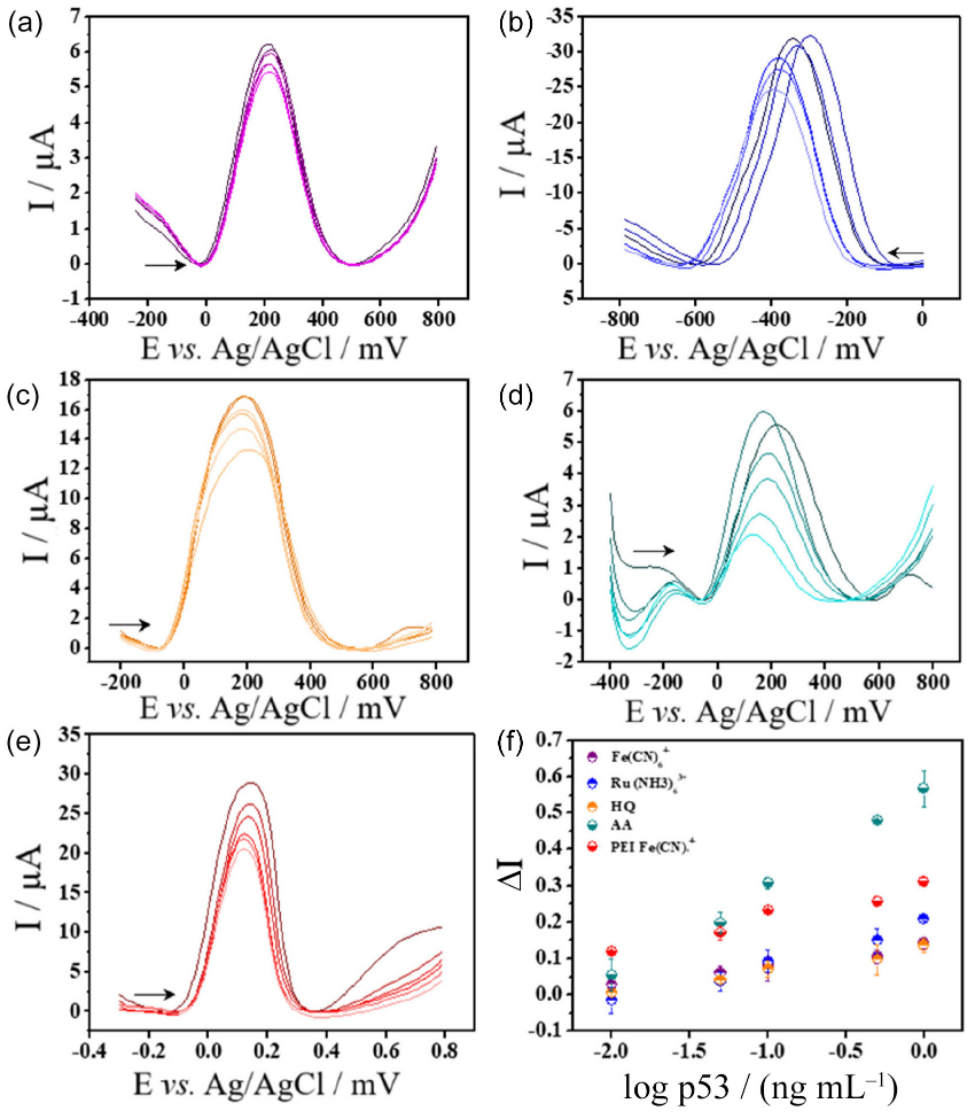

Figure 2. Voltammograms for SPCE-Pre/Ab/BSA after incubation with different concentrations of p53 (a-d). The electrochemical measurements were made in 1.0×10^{-3} mol L^{-1} of $Fe(CN)_6^{3-/4-}$ (a), $Ru(NH_3)_6^{2+/3+}$ (b), HQ (c) and AA (d) in 0.1 mol L^{-1} PB (pH 7.0). Voltammograms at different concentrations of p53 in SPCE-Pre/PEI/Ab/BSA in 1.0×10^{-3} mol L^{-1} of $Fe(CN)_6^{3-/4-}$ in 0.1 mol L^{-1} PB (pH 7.0) (e). Comparison of the analytical curves for the voltammograms in Figures a-e (f).

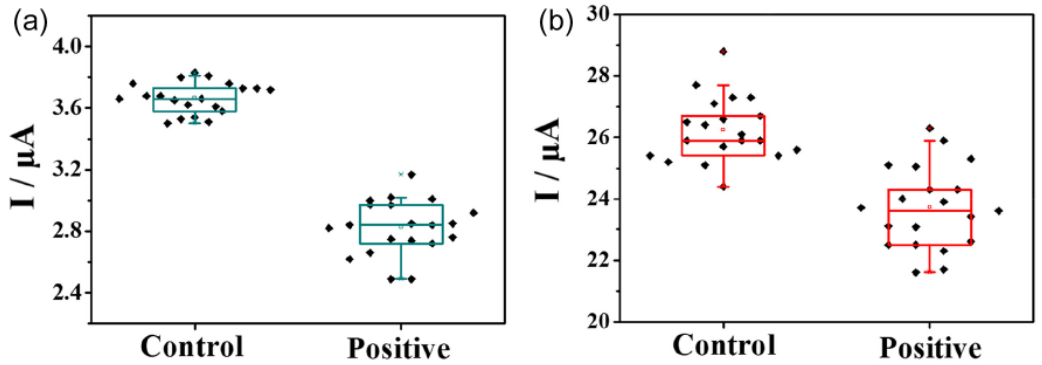

Figure 3. Box plot for the distribution of peak current intensity in voltammograms for control and positive samples analyzed with the immunosensors: (a) SPCE-Pre/Ab/BSA with AA and (b) SPCE-Pre/PEI/Ab/BSA with $Fe(CN)_6^{3-/4-}$.

features from the original dataset (identified through mutual inclusion) that contribute to the separation of the two classes. As shown in Table S1, these features correspond to current values in the region from −732 to 792 mV. Though these currents are measured far from the peak potential, they also change with p53 concentration.

Table 1. ASW values for clustering with the KM, HAC and SC algorithms. The best results for each biosensor are highlighted

Dataset	KM	HAC	SC
AA-raw	0.395	0.413	0.359
AA-mi	0.796	0.796	0.796
AA-peak	0.841	0.841	0.133
AA-stats	0.523	0.527	0.527
PEI-raw	0.391	0.391	0.369
PEI-mi	0.643	0.642	0.642
PEI-peak	0.429	0.344	0.429
PEI-stats	0.501	0.460	0.514

ASW: average silhouette width; KM: K-means; HAC: hierarchical agglomerative clustering; SC: spectral clustering; AA: ascorbic acid; PEI: polyethylene amine; AA-mi and PEI-mi: datasets generated by feature selection based on mutual information; AA-stats and PEI-stats datasets constructed considering statistical features from the voltammograms; AA-peak and PEI-peak datasets obtained using features from peak current.

Table 2 shows the average accuracy obtained from various datasets using LR, LDA, SVML, GNB, KNN, and DT algorithms. In almost all cases, the AA system demonstrated higher accuracy, ranging from 95.0 to 100.0%. This is not unexpected, given the AA system superior analytical sensitivity, which is approximately 2.4 times higher than that of the PEI system. Accuracies for the PEI system classifications ranged from 72.5 to 100%. The best performance was achieved using the PEI-stats dataset in combination with the LDA algorithm. Additionally, notable results were observed for the PEI-raw dataset when employing the LDA and SVML algorithms, yielding accuracies of 97.5%. These findings suggest that the incorporation of additional information contained in the voltammograms, coupled with machine learning-based data analysis, can significantly enhance the detection performance of electrochemical immunosensors. They are consistent with previous results[13] for the detection of SARS-CoV-2 spike protein using sandwich-type immunosensors and data analysis with SVM.

While the results obtained from this study provide valuable insights into strategies for data analysis that can significantly enhance the performance of electrochemical immunosensors, there are still opportunities for improving the applicability of such strategies in real scenarios. A key limitation of this study is the size of the dataset, which was derived from spiked artificial matrices that may not fully capture the complexities of real biological samples, where interfering substances can introduce variability and complicate the analysis. Testing the proposed methodologies on larger datasets with biological samples is essential for future studies, as it will enhance the robustness and applicability of machine learning techniques in electrochemical biosensing, ultimately leading to more reliable diagnostic tools.

Conclusions

In this study, we have demonstrated that the detection capability of electrochemical immunosensors based on voltammetric measurements can be significantly enhanced, even without the use of sophisticated materials and amplification strategies. Our investigation focused on assessing the influence of different redox probes, namely ascorbic acid (AA), hydroquinone (HQ), hexaminеruthenium(III) chloride ($Ru(NH_3)_6^{2+/3+}$), and potassium hexacyanoferrate(II) ($Fe(CN)_6^{3-/4-}$), on the analytical sensitivity of electrochemical immunosensors for detecting the p53 protein. The best results were achieved

Table 2. Average accuracy (standard deviation) of the classification with the algorithms employed. The best results for the PEI-based biosensor are highlighted

Dataset	LR	LDA	SVML	GNB	KNN	DT
AA-raw	100.0 (± 0.0)	100.0 (± 0.0)	100.0 (± 0.0)	100.0 (± 0.0)	100.0 (± 0.0)	100.0 (± 0.0)
AA-mi	100.0 (± 0.0)	100.0 (± 0.0)	100.0 (± 0.0)	100.0 (± 0.0)	100.0 (± 0.0)	100.0 (± 0.0)
AA-peak	95.0 (± 2.2)	100.0 (± 0.0)	95.0 (± 2.2)	100.0 (± 0.0)	97.5 (± 1.6)	100.0 (± 0.0)
AA-stats	97.5 (± 1.6)	100.0 (± 0.0)	100.0 (± 0.0)	100.0 (± 0.0)	100.0 (± 0.0)	100.0 (± 0.0)
PEI-raw	95.0 (± 2.2)	97.5 (± 1.6)	97.5 (± 1.6)	95.0 (± 2.2)	92.5 (± 2.6)	87.5 (± 3.3)
PEI-mi	90.0 (± 3.0)	87.5 (± 3.3)	92.5 (± 2.6)	90.0 (± 3.0)	92.5 (± 2.6)	80.0 (± 4.0)
PEI-peak	80.0 (± 4.0)	80.0 (± 4.0)	80.0 (± 4.0)	80.0 (± 4.0)	72.5 (± 4.5)	62.5 (± 4.8)
PEI-stats	92.5 (± 2.6)	100.0 (± 0.0)	97.5 (± 1.6)	92.5 (± 2.6)	95.0 (± 2.2)	92.5 (± 2.6)

LR: logistic regression; LDA: linear discriminant analysis; SVML: support vector machine with linear kernel; GNB: Gaussian Naive-Bayes; KNN: K-nearest neighbor; DT: decision trees; AA: ascorbic acid; PEI: polyethylene amine; AA-mi and PEI-mi: datasets generated by feature selection based on mutual information; AA-stats and PEI-stats datasets constructed considering statistical features from the voltammograms; AA-peak and PEI-peak datasets obtained using features from peak current.

with AA as the redox probe, likely attributed to its strong interaction with proteins (antibodies and p53), impeding its diffusion to the electrode surface. In addition, the analytical performance of the immunosensor with AA surpassed that of devices where the working electrode was modified with polyethyleneimine films. This observation emphasizes the possible advantage of selecting an appropriate redox probe over modifying the working electrode to enhance the analytical signal. Moreover, our study demonstrated that the detection performance of immunosensors can be further improved by exploiting additional information contained in the voltammograms, beyond solely relying on peak current values as commonly practiced. To achieve this, we employed supervised machine learning techniques to analyze data obtained from biosensors exposed to p53 and control samples. Each system was evaluated using four datasets constructed through different criteria for extracting features from the original voltammograms. Remarkably, biosensors with initially inferior detection capabilities can achieve performance on par with devices possessing superior analytical characteristics when the most suitable features and algorithms are employed. This highlights the significance of combining appropriate features and algorithms to optimize the performance of immunosensors.

Supplementary Information

Supplementary information (description of the datasets used in the study, cyclic voltammograms for characterization and scan rate studies, and data visualization) is available free of charge at http://jbcs.sbq.org.br as PDF file.

Acknowledgments

This work was supported by the National Institute of Organic Electronics (INEO) and the Brazilian agencies Coordenação de Aperfeiçoamento de Pessoal de Nível Superior (CAPES), Conselho Nacional de Desenvolvimento Científico e Tecnológico (CNPq), and Fundação de Amparo à Pesquisa do Estado de São Paulo (FAPESP, 2018/22214-6, 2020/09835-1).

References

1. Jones, A. L.; Dhanapala, L.; Baldo, T. A.; Sharafeldin, M.; Krause, C. E.; Shen, M.; Moghaddam, S.; Faria, R. C.; Dey, D. K.; Watson, R. W.; Andrawis, R.; Lee, N. H.; Rusling, J. F.; *Anal. Chem.* **2021**, *93*, 1059. [Crossref]
2. Cui, F.; Yue, Y.; Zhang, Y.; Zhang, Z.; Zhou, H. S.; *ACS Sens.* **2020**, *5*, 3346. [Crossref]
3. Christinelli, W. A.; Shimizu, F. M.; Facure, M. H. M.; Cerri, R.; Oliveira, O. N.; Correa, D. S.; Mattoso, L. H. C.; *Sens. Actuators, B* **2021**, *336*, 129696. [Crossref]
4. Bao, Q.; Li, G.; Cheng, W.; Yang, Z.; Qu, Z.; Wei, J.; Lin, L.; *RSC Adv.* **2023**, *13*, 23788. [Crossref]
5. Braz, D. C.; Popolin Neto, M.; Shimizu, F. M.; Sá, A. C.; Lima, R. S.; Gobbi, A. L.; Melendez, M. E.; Arantes, L. M. R. B.; Carvalho, A. L.; Paulovich, F. V.; Oliveira, O. N.; *Talanta* **2022**, *243*, 123327. [Crossref]
6. Coatrini-Soares, A.; Coatrini-Soares, J.; Popolin Neto, M.; de Mello, S. S.; Pinto, D. D. S. C.; Carvalho, W. A.; Gilmore, M. S.; Piazzetta, M. H. O.; Gobbi, A. L.; Brandão, H. M.; Paulovich, F. V.; Oliveira, O. N.; Mattoso, L. H. C.; *Chem. Eng. J.* **2023**, *451*, 138523. [Crossref]
7. Wijaya, D. R.; Afianti, F.; Arifianto, A.; Rahmawati, D.; Kodogiannis, V. S.; *Sens. Bio-Sens. Res.* **2022**, *36*, 100495. [Crossref]
8. Barauna, V. G.; Singh, M. N.; Barbosa, L. L.; Marcarini, W. D.; Vassallo, P. F.; Mill, J. G.; Ribeiro-Rodrigues, R.; Campos, L. C. G.; Warnke, P. H.; Martin, F. L.; *Anal. Chem.* **2021**, *93*, 2950. [Crossref]
9. Ortiz-Aguayo, D.; de Wael, K.; *J. Electroanal. Chem.* **2021**, *902*, 115770. [Crossref]
10. de Wael, K.; Ortiz-Aguayo, D.; Cetó, X.; Del Valle, M.; *Sens. Actuators, B* **2022**, *357*, 131345. [Crossref]
11. Enginler, S. Ö.; Küçükdeniz, T.; Dal, G. E.; Yıldırım, F.; Cilasun, G. E.; Alkan, F. Ü.; Gürgen, H. Ö.; Taşaltın, N.; Sabuncu, A.; Yılmaz, M.; Karakuş, S.; *Anal. Bioanal. Chem.* **2024**, *416*, 5071. [Crossref]
12. Tumrani, S. H.; Soomro, R. A.; Thabet, H. K.; Karakuş, S.; El-Bahy, Z. M.; Küçükdeniz, T.; Khoso, S.; *Talanta* **2024**, *278*, 126507. [Crossref]
13. Fortunati, S.; Giliberti, C.; Giannetto, M.; Bolchi, A.; Ferrari, D.; Donofrio, G.; Bianchi, V.; Boni, A.; de Munari, I.; Careri, M.; *Biosensors* **2022**, *12*, 426. [Crossref]
14. Sen, E.; Gönüllü, U.; Akar, N.; *Tuberkuloz ve Toraks* **2005**, *53*, 231. [Link] accessed in February 2025
15. Warnakulasuriya, S.; Soussi, T.; Maher, R.; Johnson, N.; Tavassoli, M.; *J. Pathol.* **2000**, *192*, 52. [Crossref]
16. Wilson, D.; Materón, E. M.; Ibáñez-Redín, G.; Faria, R. C.; Correa, D. S.; Oliveira, O. N.; *Talanta* **2019**, *194*, 611. [Crossref]
17. Brazaca, L. C.; Imamura, A. H.; Gomes, N. O.; Almeida, M. B.; Scheidt, D. T.; Pereira, P. A. R.; Oliveira, O. N.; Janegitz, B. C.; Machado, S. A. S.; Carrilho, E.; *Anal. Bioanal. Chem.* **2022**, *414*, 5507. [Crossref]
18. Nelis, J. L. D.; Migliorelli, D.; Mühlebach, L.; Generelli, S.; Stewart, L.; Elliott, C. T.; Campbell, K.; *Talanta* **2021**, *228*, 122215. [Crossref]
19. Mccreery, R. L.; *Chem Rev.* **2008**, *108*, 2646. [Crossref]
20. Wong, C. H. A.; Ambrosi, A.; Pumera, M.; *Nanoscale* **2012**, *4*, 4972. [Crossref]

21. Ferrari, A. G. M.; Foster, C. W.; Kelly, P. J.; Brownson, D. A. C.; Banks, C. E.; *Biosensors* **2018**, *8*, 53. [Crossref]
22. Peltola, E.; Aarva, A.; Sainio, S.; Heikkinen, J. J.; Wester, N.; Jokinen, V.; Koskinen, J.; Laurila, T.; *Phys. Chem. Chem. Phys.* **2020**, *22*, 16630. [Crossref]
23. Ibáñez-Redín, G.; Wilson, D.; Gonçalves, D.; Oliveira, O. N.; *J. Colloid Interface Sci.* **2018**, *515*, 101. [Crossref]
24. Orzari, L. O.; de Freitas, R. C.; Andreotti, I. A. A.; Gatti, A.; Janegitiz, B. C.; *Biosens. Bioelectron.* **2019**, *138*, 111310. [Crossref]
25. Duda, R. O.; Hart, P. E.; *Pattern Classification and Scene Analysis*; 1st ed.; Wiley: Hoboken, NJ, USA, 1973.
26. Goldberger, J.; Roweis, S.; Hinton, G.; Salakhutdinov, R.; *Adv. Neural Inf. Process. Syst.* **2005**, *17*, 513. [Link] accessed in March 2025
27. Paulovich, F. V.; Moraes, M. L.; Maki, R. M.; Ferreira, M.; Oliveira Jr., O. N.; de Oliveira, M. C. F.; *Analyst* **2011**, *136*, 1344. [Crossref]
28. Webb, A.; *Statistical Pattern Recognition*, 2nd ed.; Wiley-Blackwell: New York, USA, 2002.
29. Ng, A. Y.; Jordan, M. I.; Weiss, Y. In *Advances in Neural Information Processing Systems 14 (NIPS 2001)*; Dietterich, T.; Becker, S.; Ghahramani, Z., eds.; MIT Press: Cambridge, MA, USA, 2001, p. 849. [Link] accessed in March 2025
30. Su, W. Y.; Wang, S. M.; Cheng, S. H.; *J. Electroanal. Chem.* **2011**, *651*, 166. [Crossref]
31. Silva, R. R.; Pereira, P. A. R.; Campos, A. M.; Wilson, D.; Otoni, C. G.; Barud, H. S.; Costa, C. A. R.; Domeneguetti, R. R.; Balogh, D. T.; Ribeiro, S. J. L.; Oliveira, O. N.; *Talanta* **2020**, *218*, 121153. [Crossref]
32. Zuaznabar-Gardona, J. C.; Fragoso, A.; *Electrochim. Acta* **2020**, *353*, 136495. [Crossref]
33. Li, X.; Wang, G.; Chen, D.; Lu, Y.; *Mol. BioSyst.* **2014**, *10*, 326. [Crossref]
34. Sun, L.; Zhang, J.; Liu, K.; *Anal. Lett.* **2007**, *40*, 3050. [Crossref]
35. Li, X.; Chen, D.; Wang, G.; Lu, Y.; *Eur. J. Med. Chem.* **2013**, *70*, 22. [Crossref]
36. Dodevska, T.; Hadzhiev, D.; Shterev, I.; *Micromachines* **2023**, *14*, 41. [Crossref]
37. Ibáñez-Redín, G.; Joshi, N.; Freitas, G.; Wilson, D.; Melendez, M. E.; *Microchim. Acta* **2020**, *187*, 619. [Crossref]
38. Yang, Z.; Chevolot, Y.; Géhin, T.; Dugas, V.; Xanthopoulos, N.; Laporte, V.; Delair, T.; Ataman-Önal, Y.; Choquet-Kastylevsky, G.; Souteyrand, E.; Laurenceau, E.; *Langmuir* **2013**, *29*, 1498. [Crossref]
39. Garg, A.; Hazra, J. P.; Sannigrahi, M. K.; Rakshit, S.; Sinha, S.; *Biophys. J.* **2020**, *118*, 720. [Crossref]
40. Brett, C.; Brett, A.; *Electrochemistry: Principles, Methods and Applications*; Oxford University Press Inc.: New York, USA, 1993.
41. Weng, X.; Liu, Y.; Xue, Y.; Wang, A. J.; Wu, L.; Feng, J. J.; *Sens. Actuators, B* **2017**, *250*, 61. [Crossref]
42. Rizwan, M.; Elma, S.; Lim, S. A.; Ahmed, M. U.; *Biosens. Bioelectron.* **2018**, *107*, 211. [Crossref]
43. Fan, H.; Zhang, Y.; Wu, D.; Ma, H.; Li, X.; Li, Y.; Wang, H.; Li, H.; Du, B.; Wei, Q.; *Anal. Chim. Acta* **2013**, *770*, 62. [Crossref]

Submitted: October 15, 2024
Published online: March 14, 2025